Structure guided mutagenesis reveals the substrate determinants of guanine deaminase

Jayanti Singh [1,2], Vandana Gaded [1,3], Aruna Bitra [1], Ruchi Anand [*,4]

Department of Chemistry, Indian Institute of Technology Bombay, Mumbai, Maharashtra 400076, India

ABSTRACT

Guanine deaminases (GDs) are essential enzymes that regulate the overall nucleobase pool. Since the deamination of guanine to xanthine results in the production of a mutagenic base, these enzymes have evolved to be very specific in nature. Surprisingly, they accept structurally distinct triazine ammeline, an intermediate in the melamine pathway, as one of the moonlighting substrates. Here, by employing NE0047 (a GD from *Nitrosomonas europaea*), we delineate the nuance in the catalytic mechanism that allows these two distinct substrates to be catalyzed. A combination of enzyme kinetics, X-ray crystallographic, and calorimetric studies reveal that GDs operate via a dual proton shuttle mechanism with two glutamates, E79 and E143, crucial for deamination. Additionally, N66 appears to be central for substrate anchoring and participates in catalysis. The study highlights the importance of closure of the catalytic loop and of maintenance of the hydrophobic core by capping residues like F141 and F48 for the creation of an apt environment for activation of the zinc-assisted catalysis. This study also analyzes evolutionarily distinct GDs and asserts that GDs incorporate subtle variations in the active site architectures while keeping the most critical active site determinants conserved.

1. Introduction

Guanine deaminases (GDs) are essential enzymes of the nucleotide metabolic pathway that catalyze the hydrolytic deamination of guanine, producing xanthine and ammonia (Nygaard et al., 2000; Yuan et al., 1999). GD reaction facilitates guanine to enter the purine degradative pathway through xanthine and helps regulate the total cellular guanylate pool (Bitra et al., 2013a; Chang et al., 2004; Gaded and Anand, 2018; Maynes et al., 2000). They are expressed in all kingdoms of life, and their expression is tightly regulated (Kumar et al., 1967; Kuzmits et al., 1980). This is mainly because GDs catalyze guanine to produce the mutagenic base xanthine, which can potentially get incorporated into the genetic material, causing aberrations (Pang et al., 2012). Clinical studies show that GDs' expression is highly tissue-specific in mammals, with GDs' activity being completely absent in lymphoid tissues, whereas a high level of expression is observed in portions of the brain, liver, and kidney (Gupta and Glantz, 1985; Ito et al., 1982; Kubo et al., 2006;

Miyamoto et al., 1982; Rossi et al., 1978; Sannomiya et al., 2006). This selective expression of GDs has made them clinically significant and led to these being used as a diagnostic marker for several diseases (Fernández et al., 2009; Kumar et al., 1967; Kuzmits et al., 1980; Seffernick et al., 2010). GDs belong to two superfamilies - amidohydrolase (AHS) and cytidine-deaminase like (CDA) superfamilies (Gaded and Anand, 2018). Most eukaryotes, especially mammalian GDs belong to the AHS superfamily, display the typical $(\beta/\alpha)_8$-barrel fold while several bacterial and pathogenic strains possess the $\alpha/\beta/\alpha$ sandwich fold, unique to the CDA superfamily (Gaded and Anand, 2018; Holm and Sander, 1997; Seffernick et al., 2010; Shek et al., 2019). This fold diversity among bacterial and human species makes them apt candidates for potential drug development (Gaded and Anand, 2018).

Most of the CDA family GDs undergo a zinc-dependent deamination reaction and are functional dimers that can be evolutionary separated into two distinct groups (Bitra et al., 2013b; Frances and Cordelier, 2020; Liaw et al., 2004). The *Bacillus subtilis* GD (bGD) group harbor an

---

active site that is constituted by amino acids from both subunits (Chang et al., 2004; Liaw et al., 2004). In contrast, in the *Nitrosomonas europaea* GD (NE0047) group, the complete active site is formed from residues participating from a single subunit (Fig. 1) (Bitra et al., 2013b). Extensive functional studies on the NE0047 class reveal that shielding of the active site from the solvent is very important for the progress of the reaction (Bitra et al., 2013b). The mechanism of shielding is diverse in both groups; NE0047 has nine amino acids that form a lid that closes and opens during the course of the reaction (Fig. 1A, B), while bGD has helices that cross over from both monomers and shield the active site (Fig. 1C, D) (Bitra et al., 2013b; Liaw et al., 2004). bGD also possesses a conserved C-terminal tyrosine/aromatic residue that is shown to be essential for activity and is proposed to help in correctly anchoring of guanine (Fig. 1D) (Bitra et al., 2013b). This residue caps the active site from the neighboring subunit and is part of the domain-swapped region that intertwines the dimeric assembly in bGD (Chang et al., 2004; Liaw

et al., 2004). Despite these active site differences, both enzymes catalyze the same substrates and have similar essential amino acids such as the zinc coordinating residues and the attacking glutamic acid (E79 in NE0047, E55 in bGD (Bitra et al., 2013b; Liaw et al., 2004) (Fig. 1E) therefore, we believe they operate via a common mechanism. A series of crystal structures of NE0047 in complex with substrate and various nucleobase and nucleoside analogues along with activity assay studies have helped to establish the structural basis of substrate specificity (Bitra et al., 2013b; Liaw et al., 2004). Corroborating ITC binding data has further shown that though NE0047 active site although accommodates other bases, it accepts only guanine as the primary substrate (Bitra et al., 2013b, 2013a). Even minor modifications like a methyl group addition, such as in 9-methylguanine are not acceptable. This is mainly because the active site was found to be extremely snug, and any modifications that increase the size of the primary scaffold result in rotation of the guanine moiety in the active site (Bitra et al., 2013a, 2013b). It
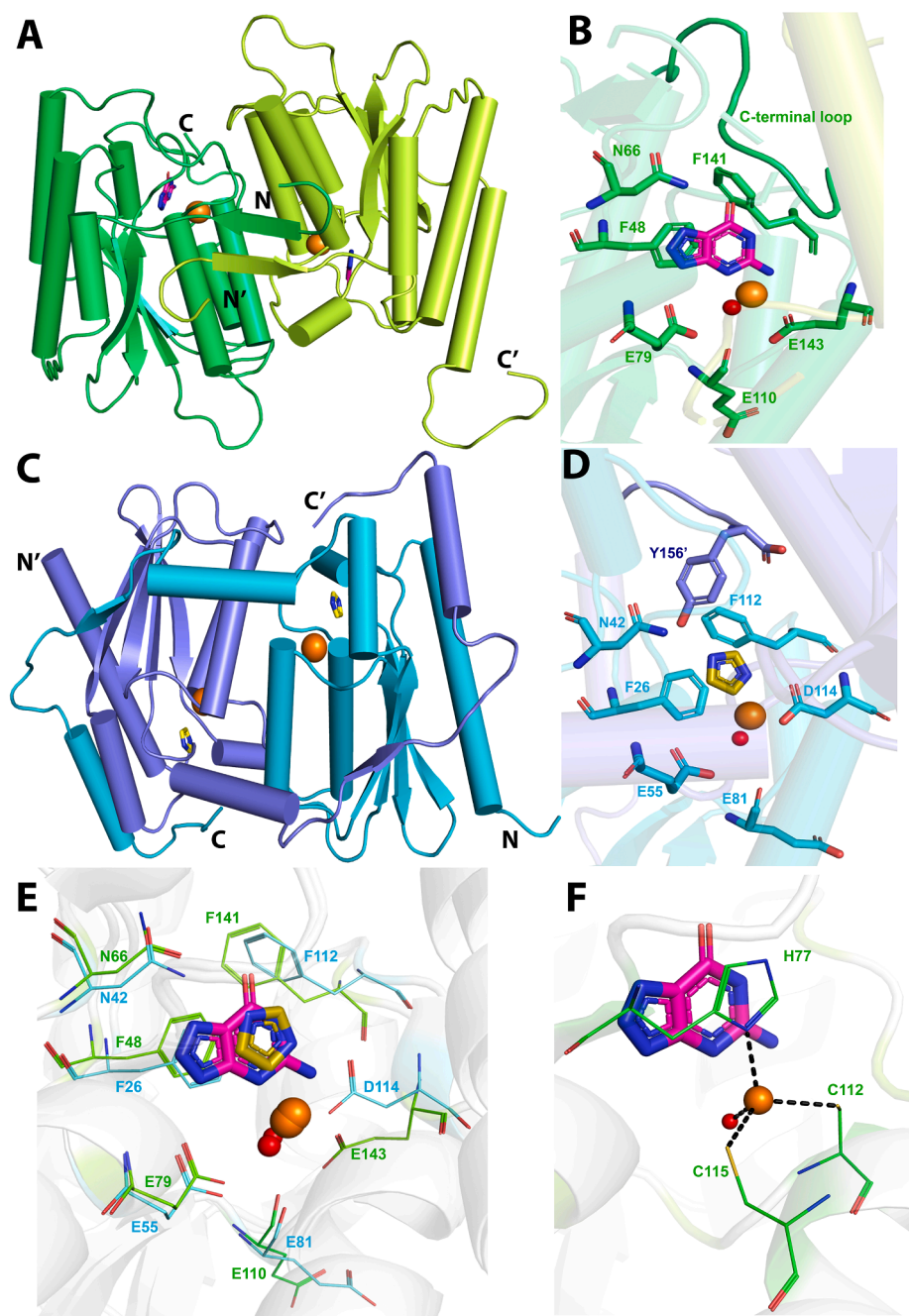
Fig. 1. Structural overview of two characterized GDs from CDA superfamily (A) Cartoon representation of NE0047 dimer (PDB ID – 4HRQ). Carbon atoms of the bound ligand (8-azaguanine) are shown in magenta (B) Close-up view of the active sites of NE0047. (C) Cartoon representation of bGD (PDB ID – 1WKQ). Carbon atoms of the bound ligand (imidazole) are shown in golden. (D) Close-up view of the active sites of bGD. (E) Active site superposition of NE0047-8-azaguanine and bGD-imidazole complex showing active site correspondence (F) Stacking interaction of 8-azaguanine with H77 which is tetrahedrally coordinated with zinc along with C112, C115 and a water molecule. Carbon atoms of the ligand binding residues of NE0047 are shown in green while that of bGD in cyan. Zinc and zinc-bound water are shown as orange and red sphere respectively.

was also shown that nucleosides such as guanosine and cytidine do not get deaminated as the closure of the C-terminal loop is impeded due to steric clashes with their ribose moiety (Bitra et al., 2013a). Surprisingly, ammeline, a triazine, is accepted by GDs as one of the moonlighting substrates. Ammeline is an intermediate in the melamine pathway, and the enzyme that deaminates it remains unknown. Reports show that even AHS superfamily enzymes, human GDs, that do not belong to the CDA superfamily and harbor completely different active site geometry, catalyze the deamination of ammeline (Seffernick et al., 2010). Therefore, it is likely not a random side substrate, and we hypothesize that GDs might serve as the primary enzyme in multiple pathways (Bitra et al., 2013b; Seffernick et al., 2010).

To further understand the requirements of catalysis and delineate how GDs catalyze the two distinct substrates guanine and ammeline, in this study, we have made significant efforts to gain insights into the basis of molecular recognition and in unraveling determinants important for deamination. To establish the role of different amino acids in the catalytic pocket, we have employed structure-guided mutagenesis, enzyme kinetics, X-ray structural, and calorimetric studies. We have solved a subset of crystal structures of NE0047 mutants in complex with 8-azaguanine (a guanine analogue) and explored the importance of key active site residues that aid in catalysis and in maintaining a hydrophobic environment during the progress of the reaction. To understand the origins of specificity, attempts to make a guanine-specific GD that does not catalyze ammeline and vice versa were also undertaken. Overall, this work helps in developing an in-depth analysis of the choice of amino acids for a particular active site cohort and provides direction towards understanding active site design in related enzyme systems.

2. Materials and methods

Mutagenesis of active site residues and enzymatic studies with mutants. The catalytic residues of NE0047 were targeted for mutagenesis, and various mutants (E79A, E143A, E143Q, E143L, F48A, F141A, N66A, N66Q, E143D, and E110A) were made by site-directed mutagenesis (Kapa Biosystems). All these mutants were expressed as six-His tag fusion proteins to facilitate purification by the standard nickel affinity chromatography method. All the procedures for protein expression and purification were the same as those described previously (Bitra et al., 2013b). The protein was concentrated to ~12 mg/mL in the sample buffer (20 mM HEPES, pH 7.5; 100 mM NaCl). The activity assay

for determining the liberation of ammonia by NE0047 mutants was performed using the Berthelot reaction as described earlier (Bitra et al., 2013b; Bonner and Cantey, 1966). The concentration of enzymes and substrates (guanine and ammeline) were maintained at 5 μM and 330 μM, respectively for activity assay. Kinetics were performed for mutants with guanine substrate concentration ranging from 30 to 200 μM as described earlier (Bitra et al., 2013b; Bonner and Cantey, 1966). The kinetic constants are listed in Table 1.

Ligand Binding experiments. NE0047 mutants were tested for affinity with 8-azaguanine and ammeline using MicroCal iTC200 (GE Healthcare, WI, USA). Samples were prepared in buffer containing 50 mM HEPES and 100 mM NaCl, pH 7.5. ITC experiments for E143D mutant were done using 20 μM protein against 0.5 mM 8-azaguanine. For F48A mutant, 30 μM protein and 1 mM 8-azaguanine were used, while 44 μM protein and 0.9 mM 8-azaguanine were used for F141A mutant. For N66A mutant, 40 μM protein was used against 4.5 mM 8-azaguanine substrate concentration. A total of 19 injections were performed for each experiment with a spacing of 180 sec between each successive injection and at a constant stirring rate of 1000 rpm. ITC experiment of E143D with ammeline was performed by adding 0.9 mM of ammeline to 100 μM of the mutant protein. The temperature was maintained at 25 °C for all the ITC experiments. To nullify the effect of heat of dilution, all the ligands were titrated against the abovementioned buffer and subtracted from the raw data prior to model fitting. The computed data is listed in Table 2.

Crystallization and structure determination of NE0047 mutants in complex with substrates. 8-azaguanine (analogue of guanine), which is also a substrate of NE0047, was used for crystallography owing to its solubility in water (Bitra et al., 2013b). Co-crystals of NE0047 (mutant)-substrate (8-azaguanine) complex were obtained in the crystallization condition consisting of 0.25 M MgCl$_2$, 25% PEG 3350, and 0.1 M Bis-Tris (pH 5.5). The obtained thin plate-like crystals were cryoprotected with a solution composed of mother liquor along with 5% glycerol, 5% sucrose, and 5% ethylene glycol and flash-cooled in liquid nitrogen. The X-ray diffraction data for all the complexes were collected at BM-14 beamline, European synchrotron radiation facility (ESRF), using 1° oscillation and 10 sec exposure time. The intensities were indexed and integrated using iMOSFLM (Battye et al., 2011). Subsequently, the intensities were scaled using the program SCALA (Project, 1994). The protein space group and unit cell parameters were similar to the earlier reported value (Bitra et al., 2013b). The structure was solved using phases from the deposited PDB entry 2G84 and further subjected to rounds of refinement using REFMAC (Murshudov et al., 1997). The crystal structure of N66A mutant clearly showed the presence of electron density (F$_o$- F$_c$ map) for 8-azaguanine at a contour level of 3σ in both the subunits. In the crystal structure of E143D mutation, the F$_o$- F$_c$ map for 8-azaguanine was visualized at a contour level of 3σ in subunit B. However, after fitting the ligand, residual positive difference peaks in the vicinity of ligand were observed, which we believe could be attributed to partial product formation as E143D enzyme mutant exhibits activity with 8-azaguanine. In subunit A (open form), ligand could not be fitted because of noise in the map. In the co-crystal structure for the N66Q mutant version of the enzyme, 8-azaguanine was present in both the subunits. The data and refinement statistics are listed in Table 3. All the figures were prepared using PyMOL (DeLano, 2020). The tilt angle of

Table 1
Kinetic parameters for various active site mutants of NE0047 towards the deamination of guanine. For E79A and E143A mutants, activity was negligible. Hence, kinetic parameters could not be computed.

NE0047 mutants	K_m (mM)	k_{cat} (s^{-1})	k_{cat}/K_m (M^{-1} s^{-1})
Native	0.12 ± 0.01	15 ± 3	$(1.2 \pm 0.3) \times 10^5$
F48A	0.43 ± 0.09	0.4 ± 0.04	$(9.1 \pm 0.7) \times 10^2$
N66A	0.42 ± 0.05	0.3 ± 0.04	$(7.1 \pm 0.3) \times 10^2$
E79A	–	–	–
F141A	1.89 ± 0.02	0.06 ± 0.02	$(3.5 \pm 0.4) \times 10^1$
E143A	–	–	–
E143D	0.35 ± 0.07	0.4 ± 0.08	$(1.1 \pm 0.5) \times 10^3$

Table 2
ITC data for binding of 8-azaguanine to various active site mutants of NE0047.

NE0047 mutants	K$_1$ (M^{-1})	ΔG$_1$ (kcal/mol)	K$_2$ (M^{-1})	ΔG$_2$ (kcal/mol)
Native	$1.4 \pm 0.3 \times 10^5$	−2.8 ± 0.5	$6.1 \pm 0.9 \times 10^3$	−4.7 ± 0.7
E143D	$1.1 \pm 0.5 \times 10^5$	−2.3 ± 0.5	$1.9 \pm 0.6 \times 10^3$	−18.7 ± 0.8
F141A	$2.3 \pm 0.2 \times 10^4$	−5.5 ± 0.4	$4.4 \pm 0.4 \times 10^3$	−6.6 ± 1.1
F48A	$8.1 \pm 0.9 \times 10^4$	−1.9 ± 0.1	$1.1 \pm 0.1 \times 10^3$	−19.9 ± 0.3
N66A	$3.4 \pm 0.4 \times 10^4$	−1.3 ± 0.3	$1.1 \pm 0.1 \times 10^3$	−3.2 ± 0.3

Table 3
Data and refinement statistics.

Protein	NE0047 (E143D)-8-azaguanine complex (PDB ID-7C3S)	NE0047 (N66A)-8-azaguanine complex (PDB ID-7C3U)	NE0047 (N66Q)-8-azaguanine complex (PDB ID-7C3T)
Space group	$P2_12_12_1$	$P2_12_12_1$	$P2_12_12_1$
Resolution (Å)	1.66	1.86	2.07
Multiplicity[a]	4.4 (4.4)	6.0 (5.6)	5.3 (4.8)
Completeness (%)[a]	99.7 (100)	99.8 (99.7)	99.3 (95.9)
Rsym (%)[a]	5.5 (48.7)	6.8 (48.4)	9.4 (47.2)
I/σ[a]	22.8 (2.4)	25.8 (3.5)	15.1 (2.78)
Total no. of reflections	166,707	158,646	104,739
No. of Unique reflections	37,813	26,490	19,828
Refinement			
Resolution range (Å)	36.3–1.66	60.8–1.86	61.3–2.07
No. of reflections total	35,915	24,122	17,682
No. of reflections test set	1889	1260	957
R_{work}/R_{free} (%)	15.6/19.2	16.5/21.7	17.8/24.2
No. of atoms			
Total	2918	2776	2748
Protein	2697	2657	2673
Ligands	38	26	22
Ion	2	2	2
Water	181	91	51
Rmsd			
Bond lengths (Å)	0.019	0.019	0.017
Bond angles (°)	1.90	1.86	1.83
Ramachandran plot			
Most favored region (%)	98.34	98.07	98.08
Additionally allowed region (%)	1.38	1.66	1.64
Outliers (%)	0.28	0.28	0.27

[a] Values in parentheses represent the data in the highest-resolution shell.

8-azaguanine in the mutant (PDB ID:7C3S**)** versus the native NE0047 (PDB ID: 4HRQ) was measured by superimposing the crystal structures in the COOT software (Emsley and Cowtan, 2004) and then comparing the slant between both the structures.

Circular Dichroism (CD) studies. CD spectra of the native NE0047 and its mutants E143Q and E143L were recorded on a Jasco J-815CD spectrometer. The protein concentration used were 0.2 mg/mL prepared in phosphate buffer (25 mM sodium phosphate pH 7.5, 80 mM NaCl). Scans were performed at 20 °C using 0.1 cm path length quartz cuvettes with 8 sec differential integration time at a scan rate of 50 nm/sec. The mean residual ellipticity (MRE) in units of $deg.cm^2.dmol^{-1}$ was determined using the formula (Kelly and Price, 2000),

$$MRE = (MRW.\theta)/10(d.c) \tag{1}$$

where θ is the observed ellipticity (degrees), d is the pathlength (cm) and c is the concentration (in units of g/ml). The MRW is obtained by dividing the molecular mass by N − 1, where N is the number of amino acids.

3. Results and discussion

Importance of proton shuttles in catalyzing GD reaction. Several structures of NE0047 with substrate analogues have provided insights into the requirements of catalysis and conformational changes that facilitate it (Bitra et al., 2013b; Seffernick et al., 2010). It is established that the deaminases undergo metal-assisted deamination (Christianson and Cox, 1999; Kunkel and Diaz, 2002; Manta et al., 2014; Seibert and Raushel, 2005), with the zinc ion in the case of NE0047 being tetrahedrally coordinated via residues C112, C115, H77 and a water molecule (Fig. 1F, S1, Scheme 1). Additionally, the role of E79 as an important nucleophile assisting zinc has been well established, and this amino acid is conserved in all nucleobase deamination reactions, whether it is cytosine, cytidine, or adenosine (Cambi et al., 1998; Ko et al., 2003; Mohamedali et al., 1996). E79, along with zinc ion, initiates deamination by activating the zinc coordinated water molecule. Here, stereo considerations regarding the optimal geometry and distance of the

carbon atom adjacent to the amino group to be deaminated from both zinc and E79 are of paramount importance. Mutation of E79 to alanine residue renders the enzyme completely inactive; this is due to the inability of alanine residue to assist in generating the Zn-hydroxide nucleophile (Fig. 2A). Besides E79 in GDs, it was proposed that another glutamic acid residue E143, also assists the reaction (Gaded and Anand, 2017; Ireton et al., 2003; Johansson et al., 2004; Losey et al., 2006). The presence of two-proton shuttles for deamination is not always the case, as the well-established cytosine deaminases whose mechanism has been studied in detail by experiment, as well as computational calculation, require only one proton shuttle (Ko et al., 2003; Sklenak et al., 2004; Yao et al., 2006, 2005). Therefore, to investigate if deamination indeed occurs via a two-proton shuttle mechanism, the other proposed proton shuttle, E143, was systematically mutated, and the effect on activity gauged (Fig. 2A). Removal of the negative charge character by mutating E143 to alanine resulted in complete loss of activity of NE0047 with both the substrates. To confirm that it was not because of unfavorable conformational changes or ineffective shielding of the active site, E143 was mutated to a similar size neutral glutamine residue (E143Q). Further to validate the significance of the electronic effect over the stereo effect towards the activity of the enzyme, leucine (E143L) mutant was also generated. Both these mutants, although folded optimally (Figure S2), were completely inactive (Fig. 2A), indicating the significance of negative charge at this position.

To further gauge the importance of the acidic head group, an E143D mutant with the same character but is one carbon length shorter than glutamic acid was engineered. Results show that the enzyme is competent and can deaminate guanine (Fig. 2A), although with a 100-fold reduction in catalytic efficiency (Table 1). ITC studies show that the ability of the enzyme to bind to the substrate is only marginally affected compared to native protein Figure S3 A, B), whereas the turnover is compromised by more than 40-fold (Tables 1 and 2). The crystal structure of the E143D mutant was solved to understand the structural basis of reduction in catalytic efficiency (Fig. 2B, C) as well as to visualize the changes in the active site introduced because of the mutation. The visualization shows that in the E143D-8-azaguanine mutant
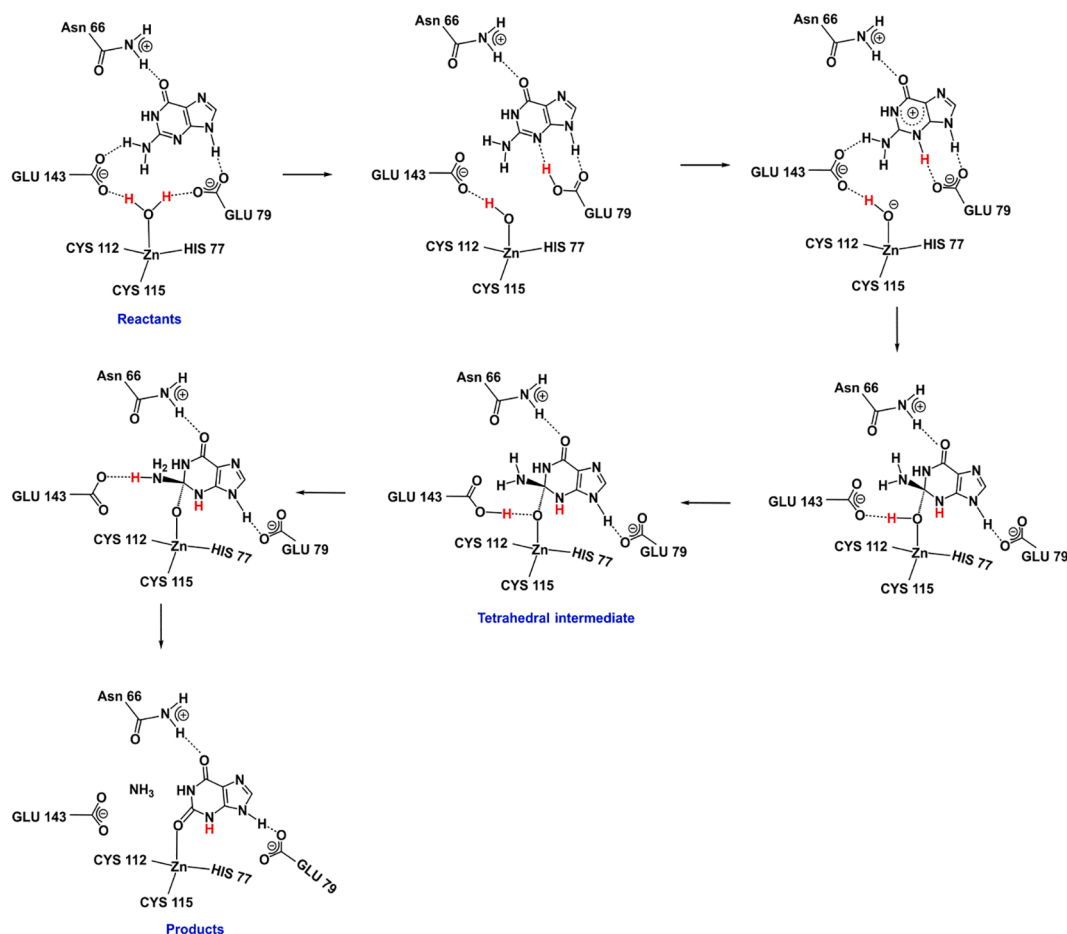
Scheme 1. Reaction mechanism proposed for the deamination of guanine by GD. Hydrogen atoms of zinc-bound water are shown in red.

structure (PDB ID-7C3S), to compensate for the shorter carbon length of aspartic acid residue, the 8-azaguanine tilts by 12°, enabling it to effectively hydrogen bond with D143 (Fig. 2C). This shift results in disruption of the stable hydrogen bonding interaction between O6 of 8-azaguanine with the amine group of N66. Asparagine at this position is a highly conserved residue that is proposed to stabilize the buildup of charge on the guanine ring during catalysis. The disruption of the H-bond in this conformation likely compromises this effect. This observation indicates that guanine is not as effectively anchored, and the interaction lost in the E143D mutation (Fig. 2C) is the prime reason the reaction rate is slowed down (Table 1). Thus, the substitution of even one amino acid can cause subtle changes in the mode of substrate binding that directly affects catalysis. However, since the basic dual proton shuttle is preserved, the enzyme is still able to deaminate guanine. In the case of E143L and E143Q mutants, in the absence of the shuttle, enzyme is unable to release ammonia and becomes incompetent, rendering it completely dead (Fig. 2A).

Based on the dual proton shuttle hypothesis, the order of the reaction mechanism can be envisaged. First, after appropriate binding of the ligand, E79 and zinc ion activate the water molecule forming a Zn-OH nucleophile that attacks the C6 carbon atom of guanine. This results in the generation of the tetrahedral intermediate state, stabilized by E79 and E143 (Scheme 1). E143 acts as an anchor that hydrogen bonds with the amino group and concurrently serves as a second proton shuttle to help release ammonia. Comparison with bGD shows that essentially, both these proton shuttles are conserved in bGD. The E79 residue of NE0047 has E55 as a counterpart in bGD, whereas E143 has D114 (Fig. 1E). In bGD as the active site is formed by both monomers, it was thought perhaps there would be differences in the mechanism. However,

the position of the proton shuttles completely overlaps with those observed in NE0047, and thus mechanistic requirements are conserved. However, due to domain swapping, the mode by which the active site occludes the solvent is slightly different; in the case of bGD, a loop that contains a conserved C-terminal tyrosine from the adjacent subunit plugs the active site, whereas, in NE0047, the C-terminal catalytic loop does the same. Even in the human GD, which has an entirely different fold and belongs to the diverse AHS superfamily, both the glutamic acids are present, and therefore these residues likely participate in the deamination via a similar route (Bitra et al., 2013b; Fernández et al., 2010; Gaded and Anand, 2018). This observation asserts that for purine deamination, two-proton shuttles are the universal operational mechanism.

The effect on the activity of the other substrate, ammeline, on perturbing position E143 was also investigated. The systematic mutation of E143 revealed that any kind of mutation at this position, including E143D, renders GD ineffective towards ammeline (Fig. 2A), one of the moonlighting substrates of the high-fidelity GD enzyme. Since the crystal structure of ammeline with E143D could not be obtained, it was superimposed in the active site using the mutant NE0047 (E143D)-azaguanine structure as a template (Fig. 2D, E). Comparison with the native NE0047-ammeline complex (PDB ID: 4LCO) indicates that one reason ammeline might be unable to get deaminated is that the replacement of glutamate by aspartate results in the amino group of ammeline to be positioned too far for D143 to participate in catalysis. Thus under these conditions, the amino group of ammeline is likely no longer hydrogen-bonded, and hence D143 cannot act as a proton shuttle (Fig. 2D, E). Further, ITC results show that E143D mutant protein does not efficiently bind to ammeline (Figure S3C); this is because the E143D
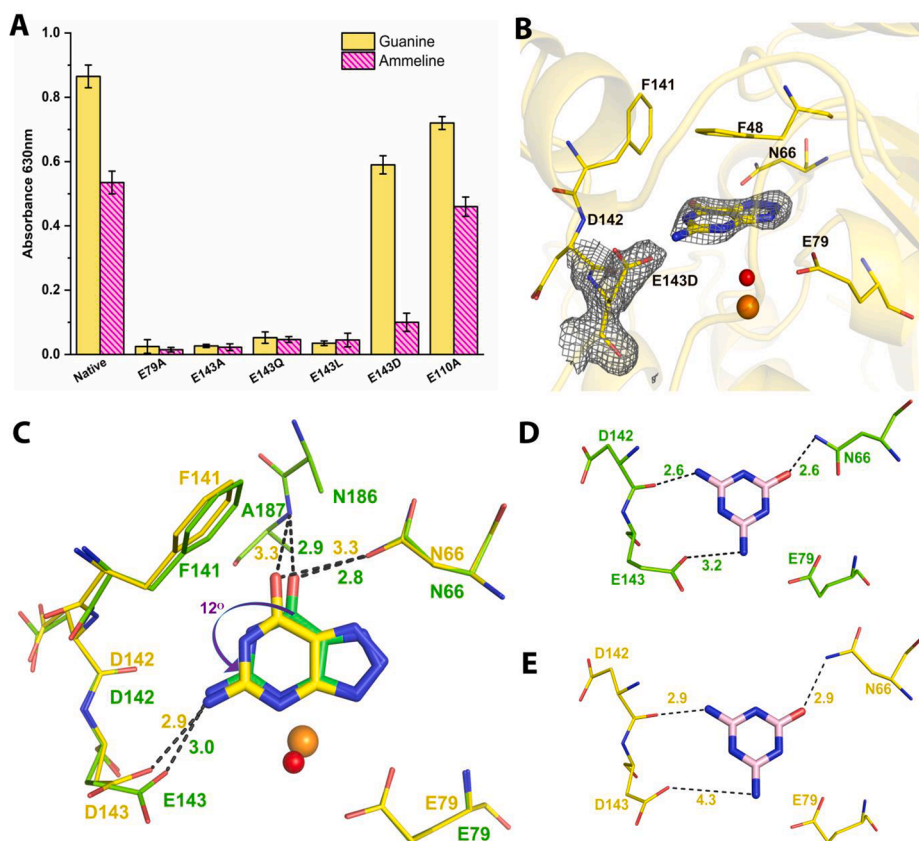
Fig. 2. Role of E143 as second proton shuttle in catalytic mechanism. (A) Activity assay of various E143 mutants of NE0047 against guanine and ammeline as substrates. (B) Crystal structure of NE0047 (E143D) in complex with 8- azaguanine to a resolution of 1.66 Å. Fo-Fc maps are contoured at 3σ for both ligand and residue. (C) Active site super-position of NE0047- 8-azaguanine and NE0047 (E143D)-8-azaguanine complex. Carbon atoms of NE0047 are shown in green and that of NE0047 mutants in yellow. Zinc atom is shown as orange sphere and the coordinated water as red sphere. (D) Active site representation of NE0047 in complex with ammeline. (E) NE0047 (E143D) mutant super-imposed with ammeline. Ammeline is shown in light pink in both D and E.
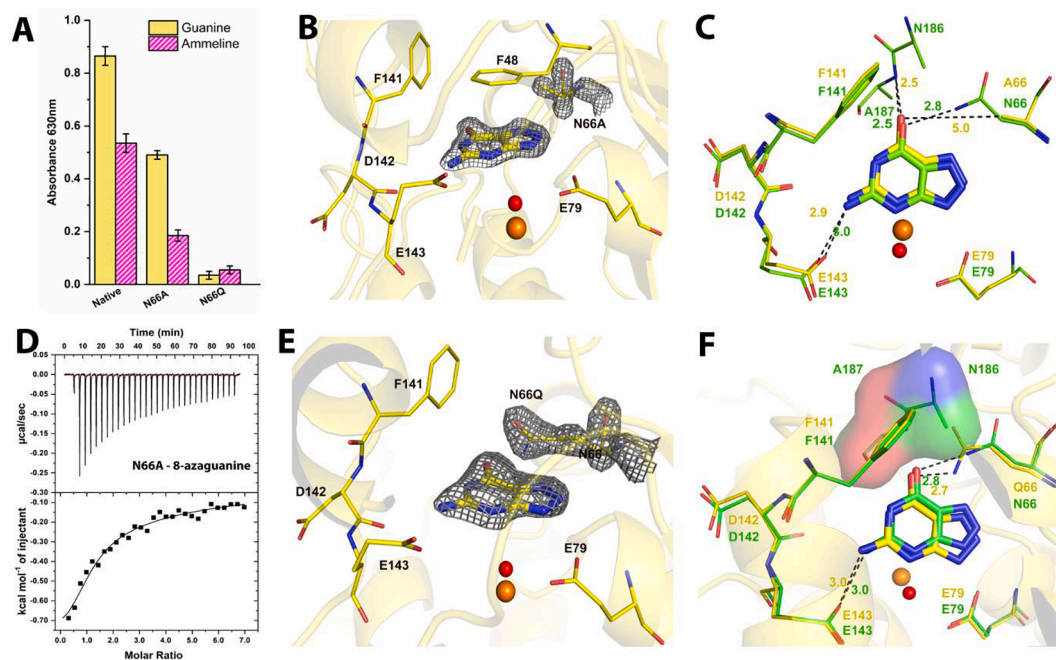

Fig. 3. Role of asparagine in stabilization and catalysis. (A) Activity assay of various N66 mutants of NE0047 against guanine and ammeline as substrates. (B) Crystal structure of NE0047 (N66Q) in complex with 8-azaguanine to a resolution of 2.07 Å. F_o-F_c maps are contoured at 3σ for both ligand and residue. (C) Active site superposition of NE0047- 8-azaguanine and NE0047 (N66A)-8-azaguanine complex. Carbon atoms of NE0047 are shown in green and that of NE0047 mutants in yellow. Zinc atom is shown as orange sphere and the coordinated water as red sphere. (D) ITC data of NE0047 (N66A) with 8-azaguanine. (E) Crystal structure of NE0047 (N66Q) in complex with 8-azaguanine to a resolution of 2.07 Å. F_o-F_c maps are contoured at 3σ for both ligand and residue. (F) Active site superposition of NE0047- 8-azaguanine and NE0047 (N66Q)-8-azaguanine complex. The clash between the C-terminal loop residue and N66Q is shown as surface representation.

mutation marginally increases the pocket size such that the enzyme is unable to stabilize ammeline, as opposed to guanine effectively; ammeline is a smaller single ring compound. The loss of activity and structural analysis reasserts that indeed E143 is an essential proton shuttle that facilitates deamination, and in the absence of this shuttle, deamination reaction cannot proceed. To further substantiate that E143D mutation was not a random charge balance effect, a control mutation, proximal E110, was mutated to alanine (Fig. 2A). This is not a central catalytic residue but is close to the active site. As expected, enzymatic activity for both guanine and ammeline was not affected by this change (Fig. 2A). Observations here highlight that E143D mutation results in a GD that preferentially catalyzes guanine, although with slightly reduced catalytic efficiency. The mutation completely abrogates ammeline activity due to its destabilization in the binding pocket.

Role of asparagine in the substrate anchoring and catalysis. The crystal structure of E143D mutant with 8-azaguanine indicated that a weakening of the hydrogen bonding interaction of guanine with N66 likely is one of the factors that affect catalytic efficiency (Table 1). To investigate this effect further, we eliminated this interaction, and the results show that the NE0047-N66A variant exhibits a 1000-fold reduction in catalytic efficiency (Table 1) towards deamination of guanine. For ammeline, the kinetic parameters could not be measured, and a low level of activity was observed (Fig. 3A). This result highlights the importance of N66 in catalysis. This residue is present in several other enzymatic reactions where purine/pyrimidine substrates are involved and aids in the stabilization of the transition state (Erion et al., 1997; Harijan et al., 2018). In fact, this residue is strictly conserved across CDA superfamily members, and, therefore, we believe it plays a central role in anchoring the substrate and plays a crucial role in catalysis in nucleobase deaminases (Gaded and Anand, 2017; Ireton et al., 2002; Iyer et al., 2011). In bGDs, one can see that this residue is conserved and structurally overlays with N66 of NE0047 (Fig. 1E). In order to understand the importance of the N66, the crystal structure of NE0047 (N66A) in a complex with 8-azaguanine was solved. Results reveal that because of

this mutation, although the guanine position is not altered, however, there is a loss of hydrogen bonding interaction that was earlier offered by the amide group of N66 (Fig. 3B, C). In the N66A mutant, the stabilization rendered via the C6 keto group of guanine is no longer viable, and because of this, the enzyme faces a higher energy barrier to facilitate the deamination leading to lower catalytic efficiency (Table 1). ITC profile also shows that the N66A mutant has a lower affinity for the substrate 8-azaguanine (Fig. 3D and Table 2). We would like to re-emphasize that for ammeline, the situation is not as debilitating as the E143D mutation, and ammeline deamination can still be catalyzed, although with significantly lower activity (Fig. 3A and Table 1). Taking together these observations, we conclude that the presence of proton shuttles is an absolute requirement for deamination, and the role of N66 is more in anchoring the substrate during catalysis.

To better understand the role of the amide nitrogen and explore how conservative changes in the active site affect activity, N66 asparagine residue was mutated to glutamine (conserving the head group nature). This mutation was performed with two different objectives. The first was to understand the effect of conserving the electronics and charge in the active site cavity by gauging the activity of the two substrates, guanine, and ammeline. The second was to engineer an enzyme that is more compact such that activity and binding of the bulkier substrate guanine can be preferentially eliminated, and the smaller substrate ammeline becomes the primary substrate. This mutation was envisaged to engineer an ammeline-specific enzyme with exclusive activity. However, to our surprise, the assay results showed that the activity was obliterated entirely for both guanine and ammeline (Fig. 3A). To investigate this observation, we solved the structure of NE0047 (N66Q)-8-azaguanine complex (Fig. 3E, F). The crystal structure with 8-azaguanine seems to indicate no anomalies. The comparison shows that with respect to the native-8-azaguanine complex, 8-azaguanine is almost precisely at the same place as in the N66A mutant complex (Fig. 3C). Both the E143 interaction and C6 keto interactions were conserved, and the guanine was accommodated in the pocket. However, to accommodate the bulkier
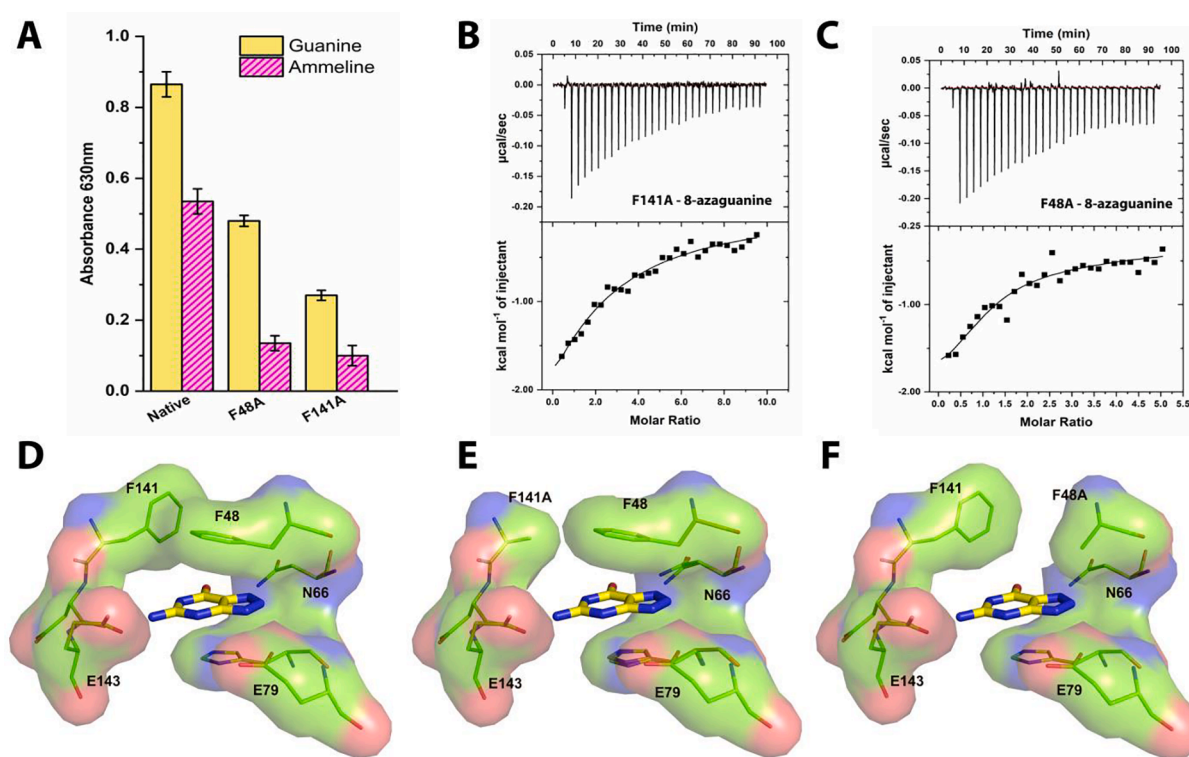
Fig. 4. Importance of hydrophobic pocket. (A) Activity assay of F48 and F141 mutants of NE0047 against guanine and ammeline as substrates. (B) ITC data of NE0047 (F141A) with 8-azaguanine. (C) ITC data of NE0047 (F48A) with 8-azaguanine. (D-F) Surface representation of active site pocket. NE0047-8-azaguanine complex (D) F141A mutant (E) F48A mutant (F).

guanine, Q66 adopts an alternate conformation. In this conformation, it does not allow the closure of the seven amino acid C-terminal catalytic loop (Bitra et al., 2013a, 2013b). This loop closes every time guanine deamination is to be initiated and creates a hydrophobic environment that allows the high-energy transition state to be achieved. In the N66Q mutant, glutamine residue causes a steric clash and interferes with the complete closure of the catalytic loop (Fig. 3F). Previous studies with other nucleoside analogue (cytidine) have also proven the importance of the closure of this loop (Bitra et al., 2013a). Reports show that although nucleoside analogues such as guanosine and cytidine were able to bind effectively and, in the case of cytidine, also adopted an optimal conformation (close to both proton shuttles), the bulky size of the substrate impeded loop closure. The nucleoside ribose sugar clashes with the catalytic loop leading to a complete loss of activity in these substrates (Bitra et al., 2013a). In N66Q, a similar scenario occurs where loop closure is impeded, which results in no activity towards both guanine and ammeline. This result highlights that every amino acid in the active site is optimized for size, shape, and electronic property. In enzymes, active sites evolve to retain activity, and the changes occur in a correlated fashion as a cohort such that the active site geometry and stereoelectronics are both conserved and the balance is maintained.

Importance of the hydrophobic pocket: To ascertain the significance of the hydrophobic cap in the zinc-assisted deamination reaction, we mutated F141 and F48 residues to alanine (Fig. 4A). These residues, along with the catalytic loop, shield the active site. Both these phenylalanine residues also provide necessary stacking interaction for proper positioning of guanine in the active site and thereby regulates the substrates' affinity (Fig. 4B, C). F141 lays on a helix-loop that is above the active site, and a 10,000-fold reduction in catalytic efficiency was observed for the F141A mutant (Table 1). ITC experiments also show lower affinity for 8-azaguanine, further validating the kinetics data (Fig. 4B, Tables 1 and 2). This residue is also completely conserved in bGD, and a comparison between bGD and NE0047 structures shows that it adopts the same conformation (Fig. 1D, E). Comparative structural analysis shows that deletion of this residue causes the active site to become slightly porous to solvent, creating a leaky active site (Fig. 4D, F). Here, the stabilization of the Zn-OH nucleophile and the tetrahedral intermediate state may become challenging to achieve thereby, slowing down the reaction tremendously. F48 residue is located internally and helps in the stabilization of the guanine moiety via π-stacking interactions. A mutation of this residue is less debilitating as compared to F141 and results in only a 1000-fold reduction in activity (Fig. 4A, B, Tables 1 and 2). Analyzing the structure, it appears that mutation of this residue creates a much smaller hole in the active site pocket, and perhaps only a few water molecules can stochastically enter from the solvent thereby, reducing the efficiency of the reaction. The mutations F141A and F48A highlight that the enzyme is sensitive to the de-shielding of the active site as this impedes activation of the zinc-bound water molecule and thus ineffective catalysis. GDs being enzymes that generate mutagen xanthine, are evolved with tight control on activity, and each and every active site amino acid is chosen to achieve perfection. A subtle interplay of residues is perfected to create effective catalysis to achieve high fidelity.

4. Conclusion

In summary, structure-guided mutagenesis of NE0047 establishes the role of active site residues in the deamination of guanine and ammeline. Studies reveal that two amino acids E79 and E143, both are essential for activity and operate by a dual proton shuttle catalytic mechanism. E143D mutation makes the enzyme selective for only guanine, and this one conservative amino acid mutation obliterates ammeline activity. N66 plays a role in anchoring and catalysis during the reaction, and this residue is optimized for size and stereoelectronics and cannot be altered without causing serious loss of function. The study also highlights the importance of catalytic loop closure and the presence of capping

residues like F141 and F48 for the creation of an apt hydrophobic environment for proper activation of the zinc coordinated water molecule, paramount for initiating the reaction.

5. Accession codes

Atomic coordinates have been deposited at the PDB with accession code 7C3U [NE0047 (N66A)-8-azaguanine], 7C3T [NE0047(N66Q)-8-azaguanine], and 7C3S [NE0047 (E143D)-8-azaguanine].

CRediT authorship contribution statement

Jayanti Singh: Data curation, Formal analysis, Investigation, Software, Visualization, Writing - review & editing. **Vandana Gaded:** Data curation, Software, Validation, Writing - original draft. **Aruna Bitra:** Conceptualization, Data curation, Formal analysis, Investigation. **Ruchi Anand:** Conceptualization, Data curation, Formal analysis, Funding acquisition, Investigation, Project administration, Resources, Supervision, Visualization, Writing - original draft, Writing - review & editing.

Declaration of Competing Interest

The authors declare that they have no known competing financial interests or personal relationships that could have appeared to influence the work reported in this paper.

Acknowledgement

This work was funded by DST, Government of India (Grant Numbers EMR/2015/002121 and DST/TM/WTI/2K16/252).

Appendix A. Supplementary data

Supplementary data to this article can be found online at https://doi.org/10.1016/j.jsb.2021.107747.

References

Battye, T.G.G., Kontogiannis, L., Johnson, O., Powell, H.R., Leslie, A.G.W., 2011. iMOSFLM: A new graphical interface for diffraction-image processing with MOSFLM. Acta Crystallogr. Sect. D Biol. Crystallogr. 67 (4), 271–281. https://doi.org/10.1107/S0907444910048675.

Bitra, A., Biswas, A., Anand, R., 2013a. Structural basis of the substrate specificity of cytidine deaminase superfamily guanine deaminase. Biochemistry 52 (45), 8106–8114. https://doi.org/10.1021/bi400818e.

Bitra, A., Hussain, B., Tanwar, A.S., Anand, R., 2013b. Identification of function and mechanistic insights of guanine deaminase from nitrosomonas europaea: role of the C-terminal loop in catalysis. Biochemistry 52, 3512–3522. https://doi.org/10.1021/bi400068g.

Bonner, W.M., Cantey, E.Y., 1966. Colorimetric method for determination of serum hyaluronidase activity. Clin. Chim. Acta. 13 (6), 746–752. https://doi.org/10.1016/0009-9981(66)90142-2.

Cambi, A., Vincenzetti, S., Neuhard, J., Vita, A., 1998. Role of glutamate-67 in the catalytic mechanism of human cytidine deaminase. Adv. Exp. Med. Biol. 431, 287–291. https://doi.org/10.1007/978-1-4615-5381-6_57.

Chang, Y.-J., Huang, C.-H., Hu, C.-Y., Liaw, S.-H., 2004. Crystallization and preliminary crystallographic analysis of Bacillus subtilis guanine deaminase. Acta Crystallogr. Sect. D Biol. Crystallogr. 60 (6), 1152–1154. https://doi.org/10.1107/S0907444904008558.

Christianson, D.W., Cox, J.D., 1999. Catalysis by metal-activated hydroxide in zinc and manganese metalloenzymes. Annu. Rev. Biochem. 68 (1), 33–57. https://doi.org/10.1146/annurev.biochem.68.1.33.

DeLano, W.L., 2020. The PyMOL Molecular Graphics System, Version 2.3. Schrödinger LLC.

Emsley, P., Cowtan, K., 2004. Coot: model-building tools for molecular graphics. Acta Crystallogr. Sect. D Biol. Crystallogr. 60 (12), 2126–2132. https://doi.org/10.1107/S0907444904019158.

Erion, M.D., Takabayashi, K., Smith, H.B., Kessi, J., Wagner, S., Hönger, S., Shames, S.L., Ealick, S.E., 1997. Purine nucleoside phosphorylase. 1. Structure−function studies †. Biochemistry 36 (39), 11725–11734. https://doi.org/10.1021/bi961969w.

Fernández, J.R., Byrne, B., Firestein, B.L., 2009. Phylogenetic analysis and molecular evolution of guanine deaminases: from guanine to dendrites. J. Mol. Evol. 68 (3), 227–235. https://doi.org/10.1007/s00239-009-9205-x.

Fernández, J.R., Sweet, E.S., Welsh, W.J., Firestein, B.L., 2010. Identification of small molecule compounds with higher binding affinity to guanine deaminase (cypin) than guanine. Bioorganic Med. Chem. 18 (18), 6748–6755. https://doi.org/10.1016/j.bmc.2010.07.054.

Frances, A., Cordelier, P., 2020. The emerging role of cytidine deaminase in human diseases: a new opportunity for therapy? Mol. Ther. 28 (2), 357–366. https://doi.org/10.1016/j.ymthe.2019.11.026.

Gaded, V., Anand, R., 2018. Nucleobase deaminases: a potential enzyme system for new therapies. RSC Adv. 8 (42), 23567–23577. https://doi.org/10.1039/C8RA04112A.

Gaded, V., Anand, R., 2017. Selective deamination of mutagens by a mycobacterial enzyme. J. Am. Chem. Soc. 139 (31), 10762–10768. https://doi.org/10.1021/jacs.7b0496710.1021/jacs.7b04967.s001.

Gupta, N.K., Glantz, M.D., 1985. Isolation and characterization of human liver guanine deaminase. Arch. Biochem. Biophys. 236 (1), 266–276. https://doi.org/10.1016/0003-9861(85)90626-5.

Harijan, R.K., Zoi, I., Antoniou, D., Schwartz, S.D., Schramm, V.L., 2018. Inverse enzyme isotope effects in human purine nucleoside phosphorylase with heavy asparagine labels. Proc. Natl. Acad. Sci. 115 (27), E6209–E6216. https://doi.org/10.1073/pnas.1805416115.

Holm, L., Sander, C., 1997. An evolutionary treasure: unification of a broad set of amidohydrolases related to urease. Proteins Struct. Funct. Genet. 28 (1), 72–82. https://doi.org/10.1002/(SICI)1097-0134(199705)28:1<72::AID-PROT7>3.0.CO;2-L.

Ireton, G.C., Black, M.E., Stoddard, B.L., 2003. The 1.14 Å crystal structure of yeast cytosine deaminase. Structure 11 (8), 961–972. https://doi.org/10.1016/S0969-2126(03)00153-9.

Ireton, G.C., McDermott, G., Black, M.E., Stoddard, B.L., 2002. The structure of Escherichia coli cytosine deaminase 1 1Edited by I. A. Wilson. J. Mol. Biol. 315 (4), 687–697. https://doi.org/10.1006/jmbi.2001.5277.

Ito, S., Takaoka, T., Nakaya, Y., Hiasa, Y., Mori, H., Tanaka, K., Ichihara, A., 1982. Clinical value of the determination of serum guanase activity. Gastroenterology 83 (5), 1102–1108. https://doi.org/10.1016/S0016-5085(82)80080-2.

Iyer, L.M., Zhang, D., Rogozin, I.B., Aravind, L., 2011. Evolution of the deaminase fold and multiple origins of eukaryotic editing and mutagenic nucleic acid deaminases from bacterial toxin systems. Nucleic Acids Res. 39, 9473–9497. https://doi.org/10.1093/nar/gkr691.

Johansson, E., Neuhard, J., Willemoës, M., Larsen, S., 2004. Structural, kinetic, and mutational studies of the zinc ion environment in tetrameric cytidine deaminase. Biochemistry 43 (20), 6020–6029. https://doi.org/10.1021/bi035893x.

Kelly, S., Price, N., 2000. The use of circular dichroism in the investigation of protein structure and function. Curr. Protein Pept. Sci. 1, 349–384. https://doi.org/10.2174/1389203003381315.

Ko, T.-P., Lin, J.-J., Hu, C.-Y., Hsu, Y.-H., Wang, A.-J., Liaw, S.-H., 2003. Crystal structure of yeast cytosine deaminase: Insights into enzyme mechanism and evolution. J. Biol. Chem. 278 (21), 19111–19117. https://doi.org/10.1074/jbc.M300874200.

Kubo, K., Honda, H., Honda, H., Sannomiya, K., Aying, Y., Mei, W., Mi, S., Aoyagi, E., Simizu, I., Ii, K., Ito, S., 2006. Histochemical and immunohistochemical investigation of guanase and nedasin in human tissues. J. Med. Investig. 53 (3,4), 264–270. https://doi.org/10.2152/jmi.53.264.

Kumar, S., Josan, V., Sanger, K.C.S., Tewari, K., Krishnan, P.S., 1967. Studies on guanine deaminase and its inhibitors in rat tissue. Biochem. J. 102, 691–704. https://doi.org/10.1042/bj1020691.

Kunkel, T.A., Diaz, M., 2002. Enzymatic cytosine deamination: friend and foe. Mol. Cell 10 (5), 962–963. https://doi.org/10.1016/S1097-2765(02)00750-5.

Kuzmits, R., Seyfried, H., Wolf, A., Müller, M.M., 1980. Evaluation of serum guanase in hepatic diseases. Enzyme 25 (3), 148–152. https://doi.org/10.1159/000459240.

Liaw, S.-H., Chang, Y.-J., Lai, C.-T., Chang, H.-C., Chang, G.-G., 2004. Crystal structure of Bacillus subtilis guanine deaminase: The first domain-swapped structure in the cytidine deaminase superfamily. J. Biol. Chem. 279 (34), 35479–35485. https://doi.org/10.1074/jbc.M405304200.

Losey, H.C., Ruthenburg, A.J., Verdine, G.L., 2006. Crystal structure of Staphylococcus aureus tRNA adenosine deaminase TadA in complex with RNA. Nat. Struct. Mol. Biol. 13, 153–159. https://doi.org/10.1038/nsmb1047.

Manta, B., Raushel, F.M., Himo, F., 2014. Reaction mechanism of zinc-dependent cytosine deaminase from Escherichia coli: a quantum-chemical study. J. Phys. Chem. B 118 (21), 5644–5652. https://doi.org/10.1021/jp501228s.

Maynes, J.T., Yuan, R.G., Snyder, F.F., 2000. Identification, expression, and characterization of Escherichia coli guanine deaminase. J. Bacteriol. 182 (16), 4658–4660. https://doi.org/10.1128/JB.182.16.4658-4660.2000.

Miyamoto, S., Ogawa, H., Shiraki, H., Nakagawa, H., 1982. Guanine deaminase from rat brain. purification, characteristics, and contribution to ammoniagenesis in the brain. J. Biochem. 91, 167–176. https://doi.org/10.1093/oxfordjournals.jbchem.a133673.

Mohamedali, K.A., Kurz, L.C., Rudolph, F.B., 1996. Site-directed mutagenesis of active site glutamate-217 in mouse adenosine deaminase. Biochemistry 35 (5), 1672–1680. https://doi.org/10.1021/bi9514119.

Murshudov, G.N., Vagin, A.A., Dodson, E.J., 1997. Refinement of macromolecular structures by the maximum-likelihood method. Acta Crystallogr. Sect. D Biol. Crystallogr. 53 (3), 240–255. https://doi.org/10.1107/S0907444996012255.

Nygaard, P., Bested, S.M., Andersen, K.A.K., Saxild, H.H., 2000. Bacillus subtilis guanine deaminase is encoded by the yknA gene and is induced during growth with purines as the nitrogen source. Microbiology 146, 3061–3069. https://doi.org/10.1099/00221287-146-12-3061.

Pang, B., McFaline, J.L., Burgis, N.E., Dong, M., Taghizadeh, K., Sullivan, M.R., Elmquist, C.E., Cunningham, R.P., Dedon, P.C., 2012. Defects in purine nucleotide metabolism lead to substantial incorporation of xanthine and hypoxanthine into DNA and RNA. Proc. Natl. Acad. Sci. 109 (7), 2319–2324. https://doi.org/10.1073/pnas.1118455109.

Project, C.C., 1994. The CCP4 suite: programs for protein crystallography. Acta Crystallogr. Sect. D Biol. Crystallogr. 50, 760–763. https://doi.org/10.1107/S0907444994003112.

Rossi, C.A., Hakim, G., Solaini, G., 1978. Purification and properties of pig brain guanine deaminase. BBA - Enzymol. 526 (1), 235–246. https://doi.org/10.1016/0005-2744(78)90308-X.

Sannomiya, K., Honda, H., Kubo, K., Ii, K., Yuan, Y., Aoyagi, E., Muguruma, N., Shimizu, I., Ito, S., 2006. A histochemical and immunohistochemical investigation of guanase and nedasin in rat and human tissues. J. Med. Investig. 53 (3,4), 246–254. https://doi.org/10.2152/jmi.53.246.

Seffernick, J.L., Dodge, A.G., Sadowsky, M.J., Bumpus, J.A., Wackett, L.P., 2010. Bacterial ammeline metabolism via guanine deaminase. J. Bacteriol. 192 (4), 1106–1112. https://doi.org/10.1128/JB.01243-09.

Seibert, C.M., Raushel, F.M., 2005. Structural and catalytic diversity within the amidohydrolase superfamily. Biochemistry 44 (17), 6383–6391. https://doi.org/10.1021/bi047326v.

Shek, R., Hilaire, T., Sim, J., French, J.B., 2019. Structural determinants for substrate selectivity in guanine deaminase enzymes of the amidohydrolase superfamily. Biochemistry 58 (30), 3280–3292. https://doi.org/10.1021/acs.biochem.9b00341.

Sklenak, S., Yao, L., Cukier, R.I., Yan, H., 2004. Catalytic mechanism of yeast cytosine deaminase: An ONIOM computational study. J. Am. Chem. Soc. 126 (45), 14879–14889. https://doi.org/10.1021/ja046462k.

Yao, L., Sklenak, S., Yan, H., Cukier, R.I., 2005. A molecular dynamics exploration of the catalytic mechanism of yeast cytosine deaminase. J. Phys. Chem. B 109 (15), 7500–7510. https://doi.org/10.1021/jp044828+.

Yao, L., Yan, H., Cukier, R.I., 2006. A combined ONIOM quantum chemical−molecular dynamics study of zinc−uracil bond breaking in yeast cytosine deaminase. J. Phys. Chem. B 110 (51), 26320–26326. https://doi.org/10.1021/jp064301s.

Yuan, G., Bin, J.C., McKay, D.J., Snyder, F.F., 1999. Cloning and characterization of human guanine deaminase. J. Biol. Chem. 274 (12), 8175–8180. https://doi.org/10.1074/jbc.274.12.8175.